ACS chemical biology

Articles

Cite This: ACS Chem. Biol. 2019, 14, 784−795

pubs.acs.org/acschemicalbiology

Deconvoluting Stress-Responsive Proteostasis Signaling Pathways for Pharmacologic Activation Using Targeted RNA Sequencing

Julia M. D. Grandjean,[†] Lars Plate,[†,‡] Richard I. Morimoto,[§] Michael J. Bollong,[‡] Evan T. Powers,[‡] and R. Luke Wiseman*[,†]

[†]Department of Molecular Medicine and [‡]Department of Chemistry, The Scripps Research Institute, La Jolla, California 92037, United States

[§]Department of Molecular Biosciences, Rice Institute for Biomedical Research, Northwestern University, Evanston, Illinois 60208, United States

Supporting Information

ABSTRACT: Cellular proteostasis is maintained by stress-responsive signaling pathways such as the heat shock response (HSR), the oxidative stress response (OSR), and the unfolded protein response (UPR). Activation of these pathways results in the transcriptional upregulation of select subsets of stress-responsive genes that restore proteostasis and adapt cellular physiology to promote recovery following various types of acute insult. The capacity for these pathways to regulate cellular proteostasis makes them attractive therapeutic targets for correcting proteostasis defects associated with diverse diseases. High-throughput screening (HTS) using cell-based reporter assays is highly effective for identifying putative activators of stress-responsive signaling pathways. However, the development of these compounds is hampered by the lack of medium-throughput assays to define compound potency and selectivity for a given pathway. Here, we describe a targeted RNA sequencing (RNAseq) assay that allows cost-effective, medium-throughput screening of stress-responsive signaling pathway activation. We demonstrate that this assay allows deconvolution of stress-responsive signaling activated by chemical genetic or pharmacologic agents. Furthermore, we use this assay to define the selectivity of putative OSR and HSR activating compounds previously identified by HTS. Our results demonstrate the potential for integrating this adaptable targeted RNAseq assay into screening programs focused on developing pharmacologic activators of stress-responsive signaling pathways.

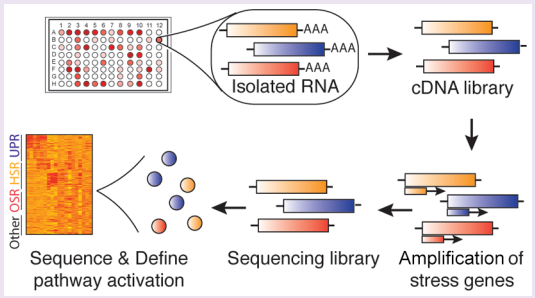

Imbalances in cellular proteostasis can be induced by genetic, environmental, or aging-related insults and are intricately involved in the pathology of multiple, etiologically diverse diseases.[1−3] These include diabetes, cardiovascular disorders, and neurodegenerative diseases such as Alzheimer's and Parkinson's disease.[1−5] To protect from these types of insults, cells have developed an integrated network of stress-responsive signaling pathways, including the heat shock response (HSR),[6−8] the oxidative stress response (OSR),[9−11] the unfolded protein response (UPR),[12−15] and the integrated stress response (ISR)[16] (Figure 1A). These pathways are activated by both distinct and overlapping types of stress and initiate signal transduction pathways that ultimately activate transcription factors such as HSR-associated heat shock factor 1 (HSF1), OSR-associated nuclear factor erythroid 2 (NRF2), and the UPR-associated transcription factors X-box binding protein 1 (XBP1s), activating transcription factor 6 (ATF6), and activating transcription factor 4 (ATF4) (the latter also being implicated in the ISR).[6−8,12,17,18] Importantly, cellular stresses can often elicit both direct and indirect activation of multiple stress-responsive signaling pathways simultaneously.[19] As a result, downstream transcription factors integrate their signaling to induce select subsets of stress-responsive genes to alleviate specific types of proteostasis stress and promote cellular recovery following an acute insult.

The capacity for these signaling pathways to protect cells against different types of proteostasis-related stress makes them highly attractive therapeutic targets for ameliorating pathologic imbalances in proteostasis associated with diverse human diseases.[1,20−25] Specifically, the activation of a single stress-responsive signaling pathway can be highly advantageous because it allows for the selective remodeling of cellular proteostasis without inducing apoptotic signaling pathways associated with global cellular stress. For example, stress-independent activation of the UPR-associated transcription factors XBP1s and ATF6 can alleviate endoplasmic reticulum (ER) stress-induced toxicity and promote secretory proteostasis of numerous disease-associated, aggregation-prone proteins, independent of pro-apoptotic signaling induced downstream of global ER stress-dependent UPR activation.[26−28] Because of the potential for stress-independent activation of these signaling pathways to influence disease, significant effort has been

Received: February 18, 2019
Accepted: March 1, 2019
Published: March 1, 2019

Downloaded via NORTHWESTERN UNIV on October 4, 2019 at 21:59:28 (UTC).
See https://pubs.acs.org/sharingguidelines for options on how to legitimately share published articles.

© 2019 American Chemical Society

DOI: 10.1021/acschembio.9b00134
ACS Chem. Biol. 2019, 14, 784−795

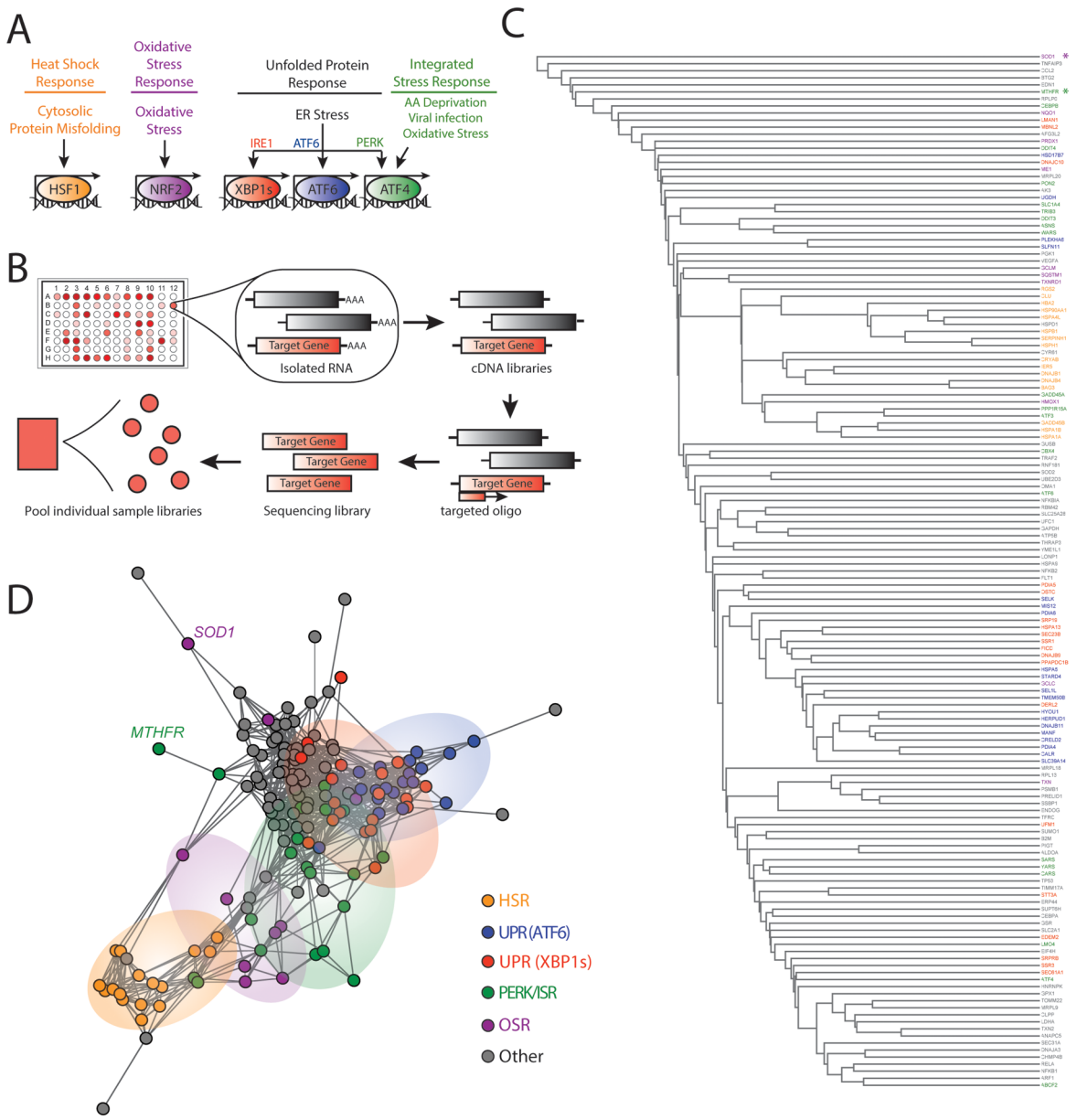

Figure 1. Targeted RNA sequencing deconvolutes stress-responsive transcriptional programs. (A) Illustration showing the stress-responsive proteostasis pathways profiled in our targeted RNAseq assay. Stresses that activate each pathway and specific transcription factors activated downstream of these pathways are also shown. (B) Schematic of the general protocol used for our targeted RNAseq assay. Briefly, RNA is isolated from cells in a 96-well plate format following a given treatment. This RNA is then converted into cDNA libraries that are probed using oligos targeted to specific stress-responsive genes (red) for sequencing library generation. Barcoded sequencing libraries from each individual treatment condition are then pooled for sequencing. (C) Dendrogram of individual target genes from our targeted RNAseq panel (see Table 1) grouped by hierarchical clustering using the Euclidean distance between each gene's expression level correlation coefficients over all treatment conditions (see Table 2 and Table S1). Genes are colored by assignment to specific stress-responsive signaling pathways to report on activation of the HSR (orange), the OSR (purple), the ATF6 UPR signaling pathway (blue), the IRE1/XBP1s UPR signaling pathway (red), the PERK/ISR signaling pathway (green), or other pathways (gray). The asterisks identify *SOD1* (purple) and *MTHFR* (green). (D) Network graph of individual target genes from our targeted RNAseq panel showing the clustering of genes into defined stress-responsive signaling pathways. This graph is derived by representing each gene as a vertex and connecting the vertices for genes whose changes in expression level correlate with Pearson $R > 0.6$. Genes that do not correlate at this level with any other genes are connected only to the gene with which they have the highest correlation coefficient. Pathways are colored using the same scheme described above in Figure 1C. *SOD1* and *MTHFR* are identified by name.

dedicated to developing highly selective pharmacologic activating compounds that target each of these pathways.

The development of these pharmacologic activators has primarily been pursued using high-throughput screening (HTS) approaches that employ cellular transcriptional reporters of target genes activated downstream of specific stress pathways, including the ATF6 signaling arm of the UPR and the HSF1-dependent HSR.[21,26,29−33] While this approach has effectively identified many putative activators of these pathways, the further development and characterization of these HTS hits are often hampered by complications, including reporter interference, a lack of compound selectivity for a given pathway, or reporter constructs not reliably reporting on activation of the entire protective transcriptional program.[25,31,34,35] Without proper

DOI: 10.1021/acschembio.9b00134
ACS Chem. Biol. 2019, 14, 784−795

Table 1. Targeted RNAseq Gene Panel for Reporting on Activation of Stress-Responsive Proteostasis Pathways

					other				
ATF6	XBP1s	PERK/ISR	HSR	OSR	hypoxic SR	NFkB	URP^{mito}	miscellaneous	
CALR	DERL2	ASNS	BAG3	GCLM	GAPDH	NFKB1	AFG3L2	ANAPC5	UFC1
CRELD2	DNAJB9	ATF3	CRYAB	HMOXI	LDHA	NFKB2	CLPP	ATP5B	ARF1
DNAJB11	ONAJC10	ATF4	CLU	PRDX1	PGK1	NFKBIA	DNAJA3	B2M	MRPL20
HERPUD1	EDEM2	ATF6	DNAJB1	SOD1	SLC2A1	RELA	ENDOG	CHMP4B	OMAI
HSPA5	HSPA13	CARS	ONAJB4	SQSTMI	TFRC	TRAF2	HSPA9	E1F4H	PRELIDI
HYOU1	LMAN1	CEBPB	GADD45B	TXNRD1	VEGFA	CCL2	LONPI	GUSB	SLC25A28
MANF	OSTC	DD1T3	HBA2	GCLC	ALDOA	ICAM1	TXN2	HNRNPK	TIMMI7A
MIS12	PD1A5	DDIT4	HSP9OAA1	NQO1	AK3	SERPINA3	YME1L1	MRPL9	TOMM22
PD1A4	PLPP5	GADD45A	HSPAIA	ME1	EDN1	TNFAIP3	HSPADI	PIGT	CEBPA
PD1A6	SEC23B	PPP1R15A	HSPA1B	TXN	FLT1	CCL5		PSMB1	ERP44
SEL1K	SEC61A1	SARS	HSPA4L					RBM42	SEC31A
SEL1L	SRP19	SLC1A4	HSPB1					RNF181	CYR61
SLC39A414	SRPRB	TR1B3	HSPH1					RPL13	MRPL18
SLFN11	SSR1	WARS	IER5					RPLP0	BTG2
TMEM50B	SSR3	YARS	RGS2					SSBP1	GPX1
UGDH	STT3A	ABCF2	SERP1NH1					SUMO1	SOD2
HSD1787	UFM1	MTHFR						SUPT6H	TP53
PLEKHA6	FICD	PON2						THRAP3	GSR
STARD4	MBNL2	LMO4						UBE2D3	
		CBX4							

tools to assess selectivity across broad stress signaling pathways, it is difficult to determine whether previous HTS has identified effective compounds that selectively activate these pathways.

One strategy for increasing the efficiency of identifying specific pathway activators from many screening hits is to incorporate upstream transcriptional profiling to first define the activation spectrum among stress-responsive signaling pathways. The benefits of this approach have been demonstrated with the recent establishment of compounds that preferentially activate the ATF6 signaling arm of the UPR, where multiplex gene expression (MGE) profiling was integrated into a screening pipeline centered on cell-based transcriptional reporters.[26] However, despite the evidence highlighting the benefit of incorporating transcriptional profiling into screening platforms, cost-effective strategies for profiling stress-responsive signaling pathway activation in a medium-throughput format are currently lacking.

Defining the magnitude and repertoire of activation among stress-responsive signaling pathways for a given stimulus is complicated by multiple challenges. Stress-responsive genes can be regulated by multiple signaling pathways, making it difficult to discern pathway activation by tracking the expression of a single gene. For example, OSR target gene *HMOX1* can be regulated by multiple stress-responsive transcription factors, including NRF2 (OSR), HSF1 (HSR), and NF-κB.[36] Furthermore, many stress-responsive signaling pathways have overlapping sets of target genes, challenging the ability to define selective activation of a certain pathway. For example, a majority of genes regulated by the UPR-associated transcription factor ATF6 are also activated, albeit to lower extents, by the alternative UPR-associated transcription factor XBP1s, thus making it difficult to deconvolute specific activation of these pathways by monitoring expression of a single gene.[28] Additionally, different stress-responsive signaling pathways induce target genes to varying extents. For example, HSF1 (HSR) target genes can be induced >10-fold more than UPR target genes.[17,28] These properties of stress-responsive signaling challenge the ability to monitor activation of specific pathways using strategies such as gene set enrichment analysis (GSEA), which is biased toward pathways that elicit stronger transcriptional responses and does not easily deconvolute overlapping stress-responsive transcriptional programs. Furthermore, GSEA requires whole transcriptome RNA sequencing (RNAseq) profiling to define pathway activation, limiting its application as a medium-throughput screening approach. One potential strategy for addressing the challenges mentioned above is to monitor activation of specified sets of stress-responsive genes regulated downstream of different stress-responsive signaling pathways, wherein pathway activation is defined by the grouped behavior for all relevant target genes. This strategy requires measuring multiple genes activated downstream of different stress-responsive signaling pathways in a cost-effective assay.

Recent advances in RNA sequencing have demonstrated the potential for this approach to be integrated into drug discovery pipelines. For example, the DRUG-seq platform established a cost-effective strategy for profiling compounds in a high-throughput format, providing a powerful approach for defining the compound mechanism of activation and selectivity.[37] However, this approach requires specialized equipment that would make it difficult to implement in most research laboratories. In contrast, the targeted RNAseq platform, described in the past 5 years (previously described as Capture-seq[38]), provides a unique opportunity to screen expression of 100−1000 genes in a cost-effective, medium-throughput format. Because this approach uses target-specific generation of sequencing libraries, targeted RNAseq demonstrates improved sensitivity for low-copy transcripts, potentially providing a larger dynamic range for tracking changes in both weakly and strongly expressed genes. Furthermore, targeted RNAseq avoids background issues caused by nonspecific probe binding or probe cross-hybridization found in technologies such as microarrays.[39] As such, this approach has been used in diverse contexts, including measuring the expression of alleles in plant populations,[40] detection of gene fusions in solid tumors,[41] and monitoring activation of cell death pathways.[42]

DOI: 10.1021/acschembio.9b00134
ACS Chem. Biol. 2019, 14, 784−795

Here, we describe a targeted RNAseq assay designed to define activation of stress-responsive proteostasis pathways in a medium-throughput format. We show that this approach allows accurate deconvolution of stress-responsive pathway activation induced by diverse chemical genetic and pharmacologic agents. Furthermore, we demonstrate the potential for this approach to define the selectivity of pharmacologic activators of stress-responsive signaling pathways by profiling the selectivity of compounds identified by high-throughput reporter screening to activate the OSR-associated transcription factor NRF2 or the HSR-associated transcription factor HSF1.[21,29] Ultimately, our results show that targeted RNAseq profiling is a highly adaptable strategy that can be efficiently incorporated into HTS pipelines and downstream compound development to improve the establishment of pharmacologic activators of specific stress-responsive signaling pathways.

RESULTS AND DISCUSSION

A Targeted RNAseq Assay for Monitoring Activation of Stress-Responsive Proteostasis Pathways. To establish a targeted RNAseq assay for monitoring activation of stress-responsive proteostasis pathways, we first defined gene sets predicted to accurately report on the activation of the predominant proteostasis pathways: the HSR, the OSR, the three signaling arms of the UPR, and the ISR (Figure 1A). We examined published transcriptional profiles using chemical genetic or pharmacologic approaches that selectively activated these stress-responsive signaling pathways in a stress-independent manner, to manually identify sets of proteostasis genes induced by each pathway. From these data, we selected 10−20 reporter genes activated downstream of the HSR,[17] the OSR,[43] and the IRE1/XBP1s, ATF6, and PERK/ATF4 signaling arms of the UPR[28,44−46] (Figure 1A and Table 1). Genes included were efficiently expressed and robustly induced by these pathways, to ensure efficient reporting in our targeted RNAseq assay. To address issues such as pathway overlap for the IRE1/XBP1s and ATF6 gene sets, we assigned genes to the pathway that elicited >75% gene activation when they were activated independently as compared to that observed during combined activation, as previously described.[28] Importantly, the gene set that reports on activation of the PERK/ATF4 signaling arm of the UPR was also used to monitor activation of the ISR, as both are activated through a process involving phosphorylation of the α subunit of eukaryotic initiation factor 2 (eIF2α) and the activity of the ATF4 transcription factor.[18,46] Stress-responsive genes activated downstream of other stress-responsive signaling pathways, including the hypoxic stress response,[47] NFκB signaling,[43,48] and the poorly defined mitochondrial unfolded protein response (UPR^{mt}),[49−51] were additionally selected from published transcriptional profiles that used stress-dependent activation of these pathways to define target gene induction. The inclusion of these genes in our gene panel improves our ability to identify compounds selective for a given proteostasis pathway. Our final gene panel consists of the 150 target genes listed in Table 1.

We used the established targeted RNAseq profiling approach with this custom gene panel to define the activation of stress-responsive signaling pathways in multiple HEK293-derived cell lines grown in 96-well plates subjected to conditions predicted to activate the different stress-responsive proteostasis pathways shown in Figure 1A (see Table 2 and Table S1). Briefly, we isolated RNA from these cells and generated cDNA libraries using a standard reverse transcriptase reaction. We then amplified our genes of interest for sequencing using targeted primer sets directed to the 150 genes in the panel (Figure 1B). Amplicons were then isolated and pooled for sequencing using the Illumina, Inc., MiSeq desktop sequencer at a target depth of 50 million paired-end reads for all pooled samples. The overall alignment of reads reflected the specific nature of this approach, with >93% of reads aligning to target regions, which is significantly greater than that observed in conventional whole transcriptome RNAseq experiments (Figure S1A). Our desktop MiSeq sequencing run yielded a median of ∼580000 reads per sample (19 conditions in triplicate, including vehicle controls for each cell line; 57 samples total), which is approximately 1% of the number of reads aligned per sample with whole transcriptome RNAseq on the same platform (approximated to 44−50 × 10^6 reads per sample). Additionally, per gene target, our targeted RNAseq assay yielded a median of 721.7 aligned reads (median total of >41000 reads) across all treatment conditions included in these analyses (Figure S1B,C). All of the data from this targeted RNAseq assay are included in Table S2.

Across replicate samples, we observed high reproducibility with all treatments demonstrating an R^2 value of >0.7 and most having an R^2 values of >0.85 (Figure S1D,E). From aligned count data, we performed unbiased clustering across all treatment conditions to determine our ability to accurately define different stress signaling pathways (Figure 1C,D and Figure S1F). This analysis shows that genes regulated by the HSR, OSR, and the three arms of the UPR (IRE1/XBP1s, ATF6, and PERK/ISR) generally cluster together, reflecting their similar regulation across the various stress conditions. However, despite this clustering, we observe significant overlap between gene sets, reflecting their integrated activation in response to diverse types of stimuli. For example, the IRE1/XBP1s (red in Figure 1D) and ATF6 (blue in Figure 1D) gene sets show significant overlap, reflecting the coordinated activation of these two pathways in response to ER stress. Furthermore, certain genes such as *SOD1*, activated downstream of the OSR-associated transcription factor NRF2,[52] separate from the OSR cluster (purple in Figure 1C,D), reflecting the ability of this gene to be regulated by multiple stress-responsive signaling pathways apart from the OSR.[53] The PERK/ISR target *MTHFR* is also regulated by other UPR signaling pathways, as well as the OSR,[54,55] and is similarly found to separate from the larger cluster of PERK/ISR targets (green in Figure 1C,D). The

Table 2. Treatment Conditions for Stress Signaling Targeted RNAseq

cell type	treatment	targeted pathway
293TcHSF1	arsenite [As(III)]	HSR/OSR/ISR
293TcHSF1	dox-HSF1	HSR
293^{DAX}	dox-XBP1s	XBP1s
293^{DAX}	DHFR-ATF6	ATF6
293^{DAX}	dox-XBP1s and DHFR-ATF6	XBP1s and ATF6
293^{DAX}	thapsigargin (Tg)	UPR
293T	thapsigargin (Tg)	UPR
293T	tunicamycin (Tm)	UPR
293T	oligomycin	lSR/OSR
293T	paraquat	lSR/OSR
293T	CBR-470-1	OSR
293T	bardoxolone	OSR
293T	A3	HSR
293T	C1	HSR
293T	D1	HSR
293T	F1	HSR

DOI: 10.1021/acschembio.9b00134
ACS Chem. Biol. 2019, 14, 784−795

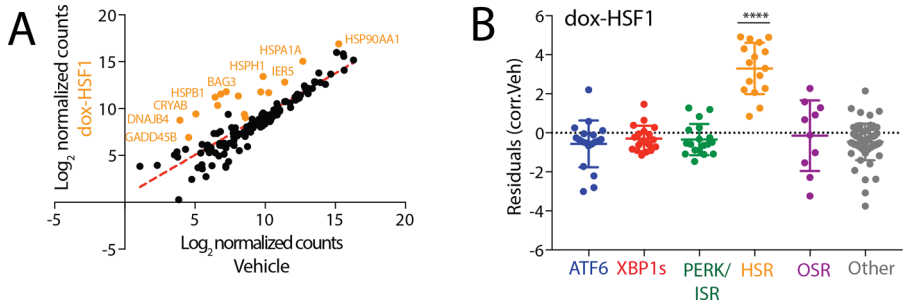

Figure 2. Targeted RNAseq accurately defines HSR activation induced by stress-independent activation of cHSF1. (A) Log_2-normalized aligned transcript counts for HEK293^{TREX} cells expressing doxycycline (dox)-inducible cHSF1 treated with 2.25 μM dox (y-axis) or vehicle (x-axis) for 16 h. Aligned transcript counts represent averages from three independent replicates quantified from our targeted RNAseq assay. All identified genes are HSR target genes. (B) Plot showing residuals calculated by comparing the expression of our panel of stress-responsive genes between HEK293^{TREX} cells expressing dox-inducible cHSF1 following treatment with dox (2.25 μM) or vehicle for 16 h. Calculation of residuals was performed as described in the legend of panel A. Statistics were calculated using one-way analysis of variance (ANOVA). The significance reflects comparison to the "other" target transcript set. $^{**}p < 0.01$, $^{***}p < 0.001$; $^{****}p < 0.0001$. See Table S3 for the full ANOVA table.

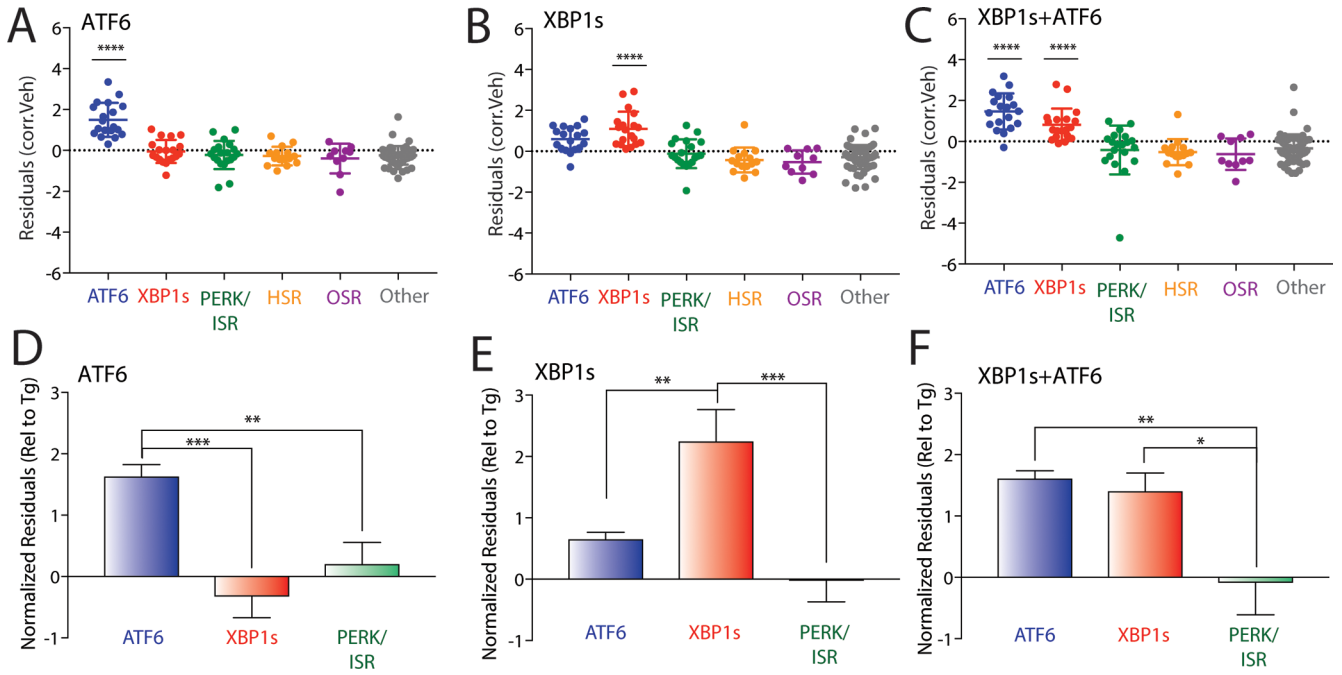

Figure 3. Targeted RNAseq defines stress-independent activation of UPR-associated signaling pathways. (A) Plot showing residuals calculated by comparing the expression of our panel of stress-responsive genes between HEK293^{DAX} cells following treatment with trimethoprim (10 μM for 4 h; activates DHFR-ATF6) or vehicle. Calculation of residuals was performed as described in the legend of Figure 2A. Statistics were calculated using one-way ANOVA. The significance reflects comparison to the "other" target transcript set. $^{****}p < 0.0001$. See Table S3 for the full ANOVA table. (B) Plot showing residuals calculated by comparing the expression of our panel of stress-responsive genes between HEK293^{DAX} cells following treatment with dox (1 μg/mL for 4 h; activates dox-inducible XBP1s) or vehicle. Calculation of residuals was performed as described in the legend of Figure 2A. Statistics were calculated using one-way ANOVA. The significance reflects comparison to the "other" target transcript set. $^{****}p < 0.0001$. See Table S3 for the full ANOVA table. (C) Plot showing residuals calculated by comparing the expression of our panel of stress-responsive genes between HEK293^{DAX} cells following treatment with both trimethoprim (10 μM for 4 h; activates DHFR-ATF6) and dox (1 μg/mL for 4 h; activates dox-inducible XBP1s) or vehicle. Calculation of residuals was performed as described in the legend of Figure 2A. Statistics were calculated using one-way ANOVA. The significance reflects comparison to the "other" target transcript set. $^{****}p < 0.0001$. See Table S3 for the full ANOVA table. (D) Graph showing normalized residuals for gene sets regulated by the ATF6 (blue), XBP1s (red), or PERK (green) UPR signaling pathways in HEK293^{DAX} cells following treatment with TMP (10 μM for 4 h; activates DHFR-ATF6). The residuals for each gene were normalized to those observed for thapsigargin (Tg)-induced ER stress in HEK293^{DAX} cells (Figure S3A,B). Normalized data were subjected to ROUT outlier testing. Statistics from one-way ANOVA. $^{**}p < 0.01$; $^{***}p < 0.001$. (E) Graph showing normalized residuals for gene sets regulated by the ATF6 (blue), XBP1s (red), or PERK (green) UPR signaling pathways in HEK293^{DAX} cells following treatment with dox (1 μg/mL for 4 h; activates dox-inducible XBP1s). The residuals for each gene were normalized to those observed for thapsigargin (Tg)-induced ER stress in HEK293^{DAX} cells (Figure S3A,B). Normalized data were subjected to ROUT outlier testing. Statistics from one-way ANOVA. $^{**}p < 0.01$; $^{***}p < 0.001$. (F) Graph showing normalized residuals for gene sets regulated by the ATF6 (blue), XBP1s (red), or PERK (green) UPR signaling pathways in HEK293^{DAX} cells following treatment with both TMP (10 μM for 4 h; activates DHFR-ATF6) and dox (1 μg/mL for 4 h; activates dox-inducible XBP1s). The residuals for each gene were normalized to those observed for thapsigargin (Tg)-induced ER stress in HEK293^{DAX} cells (Figure S3A,B). Normalized data were subjected to ROUT outlier testing. Statistics from one-way ANOVA. $^{*}p < 0.05$; $^{**}p < 0.01$.

DOI: 10.1021/acschembio.9b00134
ACS Chem. Biol. 2019, 14, 784−795

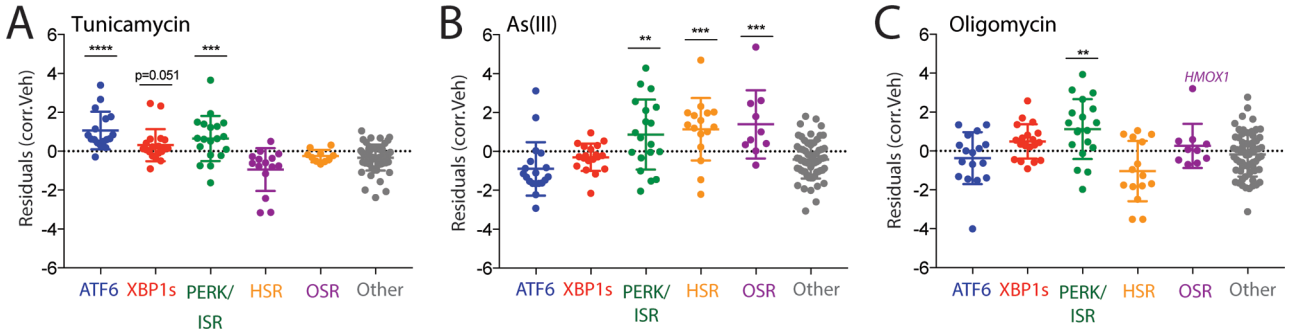

Figure 4. Targeted RNASeq profiling defines activation of stress-responsive signaling pathways induced by diverse environmental toxins. (A) Plot showing residuals calculated by comparing the expression of our stress-responsive gene panel between HEK293T cells following treatment with tunicamycin (Tm; 10 μM for 4 h) or vehicle. Calculation of residuals was performed as described in the legend of Figure 2A. Genes are grouped by target stress-responsive signaling pathway. Statistics were calculated using one-way ANOVA. The significance reflects comparison to the "other" target transcript set. ***$p < 0.001$; ****$p < 0.0001$. See Table S3 for the full ANOVA table. (B) Plot showing residuals calculated by comparing the expression of our stress-responsive gene panel between HEK293T cells following treatment with arsenite [As(III); 25 μM for 16 h] or vehicle. Calculation of residuals was performed as described in the legend of Figure 2A. Genes are grouped by target stress-responsive signaling pathway. Statistics were calculated using one-way ANOVA. The significance reflects comparison to the "other" target transcript set. **$p < 0.01$; ***$p < 0.001$. See Table S3 for the full ANOVA table. (C) Plot showing residuals calculated by comparing the expression of our stress-responsive gene panel between HEK293T cells following treatment with oligomycin A (Oligo; 100 nM for 24 h) or vehicle. Calculation of residuals was performed as described in the legend of Figure 2A. Genes are grouped by target stress-responsive signaling pathway. Statistics were calculated using one-way ANOVA. The significance reflects comparison to the "other" target transcript set. **$p < 0.01$. See Table S3 for the full ANOVA table.

overlap of gene sets and promiscuity for specific genes to report on multiple pathways highlights the importance of tracking sets of stress-responsive genes for defining overall pathway activation. However, the general clustering of our stress pathway gene sets indicates that this targeted RNAseq assay is capable of tracking changes in stress-responsive genes to accurately define activation of specific stress-responsive signaling pathways.

Defining Stress-Independent HSR and UPR Signaling Pathways through Targeted RNAseq Profiling. We initially validated the ability for our targeted RNAseq assay to report on activation of specific stress signaling proteostasis pathways using chemical genetic approaches that allow activation of specific pathways independent of stress. First, we defined activation of the HSR-regulated proteostasis genes in HEK293^{TREX} cells following doxycycline (dox)-dependent activation of a constitutively active HSF1 (cHSF1),[17] the primary transcription factor regulated by the HSR.[6−8] To define the induction of specific target proteostasis genes in our targeted RNAseq data, we first median-normalized aligned counts per target gene across all treatment conditions. We took average normalized count values across sample replicates and performed a $\log_2$ transformation, yielding the "$\log_2$-normalized counts" used for relative expression analysis. To compare chemical genetic and pharmacologic activating conditions versus vehicle control samples, we conducted a linear regression of $\log_2$-normalized counts to yield a line of best fit (Figure 2A), reflecting baseline expression levels for the majority of genes not affected by a given treatment. We then calculated the deviation of each target gene for the experimental condition from the line of best fit, or "residual value", which was used to quantify up- and downregulation of that gene (Figure 2A). Finally, we define pathway activation by plotting the residual values of each gene from this analysis, grouped according to the assigned stress-responsive pathway, and monitoring the overall behavior of the gene set (Figure 2B). This allows us to normalize variability in gene induction across different treatments and minimize challenges associated with weakly expressed genes that show high levels of induction. From this analysis, we demonstrate that dox-dependent cHSF1 activation robustly and selectively activates the entire target HSR-regulated proteostasis program, thus confirming the ability for our targeted RNAseq assay to define activation of this pathway (Figure 2B and Table S3). Interestingly, the activation of this pathway is identical to that observed when we perform the same analysis using published RNAseq transcriptional profiles for dox-dependent cHSF1 activation,[17] demonstrating that our RNAseq assay accurately quantifies the induction of HSR-regulated proteostasis target genes (Figure S2A−C).

A significant challenge in monitoring activation of stress-responsive signaling pathways is the overlap between closely related pathways. For example, the IRE1/XBP1s UPR pathway induces expression of multiple genes also regulated by the ATF6 UPR signaling pathway, albeit to lower extents.[28] Furthermore, other XBP1s target genes are often induced to levels lower than that observed for ATF6-selective target genes.[28] To define the potential for targeted RNAseq to discern selective activation of these two UPR signaling pathways, we performed this assay in HEK293^{DAX} cells subjected to stress-independent XBP1s and/or ATF6 activation. HEK293^{DAX} cells express dox-inducible XBP1s and trimethoprim (TMP)-regulated DHFR-ATF6, allowing activation of these two transcription factors in the same cell independent of ER stress through administration of dox and/or TMP.[28] As a control, we also monitored gene expression in response to global ER stress induced by treating HEK293^{DAX} cells with the SERCA pump inhibitor, thapsigargin (Tg). As expected, Tg treatment showed robust activation of all three UPR signaling pathways (IRE1/XBP1s, ATF6, and PERK/ISR), confirming global UPR activation (Figure S3A,B). In contrast, TMP-dependent DHFR-ATF6 activation showed significant increases in the ATF6 target gene set, consistent with selective ATF6 activation (Figure 3A). However, dox-inducible XBP1s increased the level of expression of both the IRE1/XBP1s and ATF6 target gene sets, although ATF6 target genes were induced less than that observed following ATF6 activation (Figure 3B), which is consistent with previous work.[28] Combined treatment with dox (activating XBP1s) and TMP (activating DHFR-ATF6) elicited a strong upregulation of both gene sets (Figure 3C).

DOI: 10.1021/acschembio.9b00134
ACS Chem. Biol. 2019, 14, 784−795

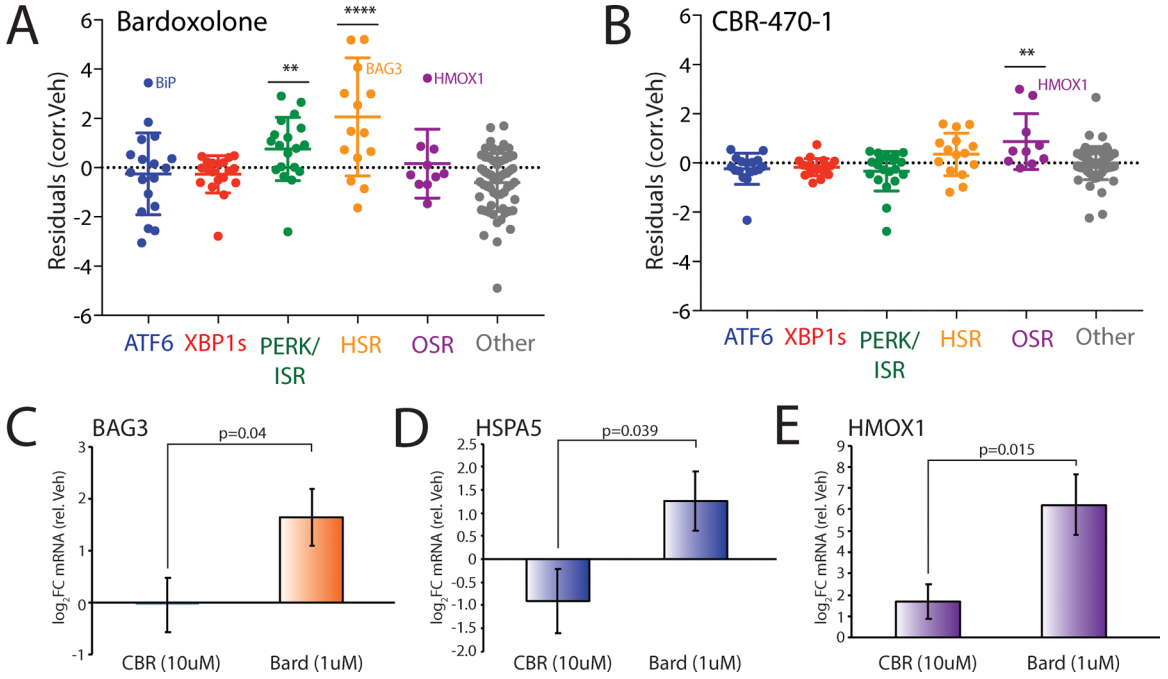

Figure 5. Defining the selectivity of the reported NRF2 activating compounds through targeted RNAseq transcriptional profiling. (A) Plot showing residuals calculated by comparing the expression of our stress-responsive gene panel between HEK293T cells treated with bardoxolone (1 μM for 24 h) or vehicle. Calculation of residuals was performed as described in the legend of Figure 2A. Genes are grouped by target stress-responsive signaling pathway. Statistics were calculated using one-way ANOVA. The significance reflects comparison to the "other" target transcript set. $^{**}p < 0.01$; $^{****}p < 0.0001$. See Table S3 for the full ANOVA table. (B) Plot showing residuals calculated by comparing the expression of our stress-responsive gene panel between HEK293T cells treated with CBR-470-1 (10 μM, 24 h) or vehicle. Calculation of residuals was performed as described in the legend of Figure 2A. Genes are grouped by target stress-responsive signaling pathway. Statistics were calculated using one-way ANOVA. The significance reflects comparison to the "other" target transcript set. $^{**}p < 0.01$. See Table S3 for the full ANOVA table. (C) Graph showing qPCR analysis of the HSR target gene *BAG3* in HEK293T cells treated for 24 h with bardoxolone (1 μM) or CBR-470-1 (10 μM). Error bars show the standard error of the mean (SEM) for three experiments. *p* values calculated using a one-tailed Student's *t* test. (D) Graph showing qPCR analysis of the UPR (ATF6) target gene *BiP* in HEK293T cells treated for 24 h with bardoxolone (1 μM) or CBR-470-1 (10 μM). Error bars show the SEM for three experiments. *p* values calculated using a one-tailed Student's *t* test. (E) Graph showing qPCR analysis of the OSR target gene *HMOX1* in HEK293T cells treated for 24 h with bardoxolone (1 μM) or CBR-470-1 (10 μM). Error bars show the SEM for three experiments. *p* values calculated using a one-tailed Student's *t* test.

Previous reports indicate that the overlap between XBP1s and ATF6 target gene expression observed following stress-independent activation could be deconvoluted by normalizing the expression of genes to that observed with Tg treatment, providing a way to sensitively define the extent of pathway activation.[26] Performing this normalization shows that TMP-dependent DHFR-ATF6 activation selectively induces expression of ATF6 target genes to levels similar to those observed for Tg-dependent ER stress (Figure 3D). Importantly, dox-dependent XBP1s activation selectively induces expression of IRE1/XBP1s target genes to levels similar to that observed with Tg by this analysis while only moderately affecting ATF6 target gene expression (Figure 3E). This profile is distinct from that observed in cells in which XBP1s and ATF6 are co-activated, which shows significantly higher levels of induction of both gene sets (Figure 3F). Importantly, when residual values from our targeted RNAseq analysis are compared to transcriptional changes from whole transcriptome RNAseq collected from HEK293^{DAX} cells subjected to XBP1s and/or ATF6 activation, there is a clear correlation between the two data sets in upregulated targets (Figure S3C–E). These results demonstrate that our targeted RNAseq assay can sensitively deconvolute the complex integration of stress-responsive signaling pathways involved in UPR signaling.

Targeted RNAseq Profiling Defines Stress Pathway Activation Induced by Cellular Toxins. We next used our targeted RNAseq assay to profile activation of stress-responsive signaling pathways induced by chemical toxins, including tunicamycin (Tm; an ER stressor that inhibits N-linked glycosylation), the environmental toxin arsenite [As(III)], the mitochondrial ATP synthase inhibitor oligomycin, and the ROS-generating compound paraquat (PQ). As predicted, our assay demonstrates that these compounds induce unique activation profiles of different stress-responsive signaling pathways. Consistent with the selective induction of ER stress, Tm treatment activates the three arms of the UPR without globally impacting other stress-responsive signaling pathways (Figure 4A). In contrast, As(III) induces robust activation of the cytosolic HSR, OSR, and ISR signaling pathways (Figure 4B), highlighting the promiscuous nature of this toxin for cytosolic proteostasis pathway activation.[56] Oligomycin treatment significantly activated only the ISR gene set, reflecting emerging evidence showing that mitochondrial stress promotes signaling through this pathway (Figure 4C).[8,50,51,57] PQ treatment also showed modest increases in ISR genes, although the entire pathway was not significantly activated (Figure S4). However, while our gene sets report on activation of whole pathways, numerous individual stress-responsive genes from multiple pathways were induced upon these different treatments. For example, the OSR target gene *HMOX1* is induced in cells treated with mitochondrial toxins oligomycin and paraquat, although we do not observe induction of other OSR target genes. Because

DOI: 10.1021/acschembio.9b00134
ACS Chem. Biol. 2019, 14, 784–795

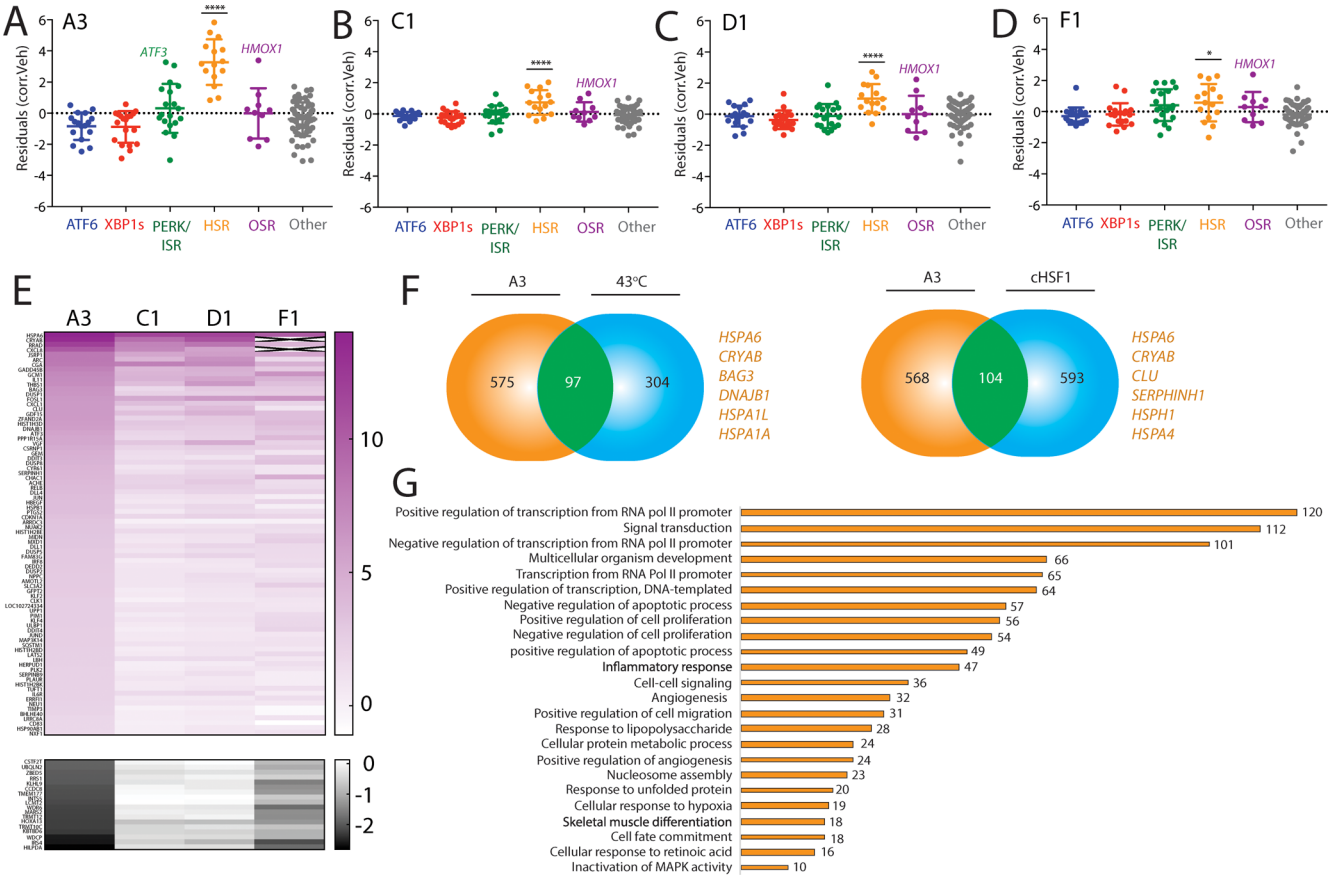

Figure 6. Defining the selectivity for HSF1 activating compounds identified through reporter-based HTS. (A) Plot showing residuals calculated by comparing the expression of our stress-responsive gene panel between HEK293T cells treated with compound A3 (10 μM for 4 h) or vehicle. Calculation of residuals was performed as described in the legend of Figure 2A. Genes are grouped by target stress-responsive signaling pathway. Statistics were calculated using one-way ANOVA. The significance reflects comparison to the "other" target transcript set. ****$p < 0.0001$. See Table S3 for the full ANOVA table. (B) Plot showing residuals calculated by comparing the expression of our stress-responsive gene panel between HEK293T cells treated with compound C1 (10 μM for 4 h) or vehicle. Calculation of residuals was performed as described in the legend of Figure 2A. Genes are grouped by target stress-responsive signaling pathway. Statistics were calculated using one-way ANOVA. The significance reflects comparison to the "other" target transcript set. ****$p < 0.0001$. See Table S3 for the full ANOVA table. (C) Plot showing residuals calculated by comparing the expression of our stress-responsive gene panel between HEK293T cells treated with compound D1 (10 μM for 4 h) or vehicle. Calculation of residuals was performed as described in the legend of Figure 2A. Genes are grouped by target stress-responsive signaling pathway. Statistics were calculated using one-way ANOVA. The significance reflects comparison to the "other" target transcript set. ****$p < 0.0001$. See Table S3 for the full ANOVA table. (D) Plot showing residuals calculated by comparing the expression of our stress-responsive gene panel between HEK293T cells treated with compound F1 (10 μM for 4 h) or vehicle. Calculation of residuals was performed as described in the legend of Figure 2A. Genes are grouped by target stress-responsive signaling pathway. Statistics were calculated using one-way ANOVA. The significance reflects comparison to the "other" target transcript set. *$p < 0.05$. See Table S3 for the full ANOVA table. (E) Heat map of fold change transcript levels from whole transcriptome RNAseq (relative to vehicle-treated cells) for the 100 genes most significantly altered by A3 treatment in HEK293T cells (82 positive regulation, top; 10 negative regulation, bottom). The changes in these genes are also shown for HEK293T cells treated with C1, D1, and F4 (10 μM for 4 h). (F) Venn diagrams showing the overlap of upregulated genes from whole transcriptome RNAseq of HEK293T cells treated with A3 (10 μM for 4 h) and HeLa cells under heat shock (left)[6] or dox-inducible cHSF1 (right) in HEK293^{TREX} cells.[17] Select genes identified in the overlap are highlighted. (G) Numbers of genes from GO analysis of significantly altered transcripts in HEK293T cells treated with compound A3 (10 μM for 4 h) relative to vehicle-treated cells. GO analysis was performed using David.[61] The entire GO analysis is reported in Table S5.

HMOX1 can be regulated by multiple stress-responsive signaling pathways,[36] these results suggest that administration of these toxins induces pleiotropic effects on multiple stress-responsive signaling pathways outside of the four primary proteostasis pathways profiled in our targeted RNAseq platform. Regardless, it is clear that our targeted RNAseq assay does accurately reflect predicted toxin-induced activation of proteostasis pathways, further validating the benefit of this approach for profiling pharmacologic activators of stress-responsive proteostasis pathways.

Defining the Selectivity of Pharmacologic NRF2 Activating Compounds through Targeted RNAseq Transcriptional Profiling. We next employed our targeted RNAseq assay to define the selectivity of two putative NRF2 activating compounds: bardoxolone and the recently described CBR-470-1 (Figure S5A).[29] Bardoxolone is an anti-inflammatory compound currently in clinical trials for chronic kidney disease. This compound is reported to induce protective benefits through activation of the OSR-associated transcription factor NRF2.[23,58] However, it also covalently modifies hundreds of proteins[59] and displays additional cellular activities, including inhibition of the mitochondrial protease LON,[60] suggesting that, apart from NRF2, bardoxolone could also activate other stress-responsive signaling pathways. Interestingly, we show in

DOI: 10.1021/acschembio.9b00134
ACS Chem. Biol. 2019, 14, 784−795

HEK293T cells that bardoxolone significantly induces expression of the OSR target gene *HMOX1* but not other OSR target genes (Figure 5A). However, this compound does induce the HSR and ISR gene sets, indicating promiscuous activity for this pharmacologic agent. Furthermore, we see strong upregulation of the ATF6 target gene *HSPA5* (also known as BiP), without complete activation of the ATF6 pathway. These results indicate that bardoxolone induces pleiotropic effects on stress-responsive genes outside of NRF2 activation in HEK293T cells. In contrast, CBR-470-1 showed selective activation of the OSR gene set with no significant induction of other stress pathways, suggesting improved selectivity of CBR-470-1 for OSR activation (Figure 5B). Consistent with this, quantitative polymerase chain reaction (qPCR) analysis of *BAG3* (an HSR target) and *HSPA5* shows that bardoxolone promiscuously induces these non-NRF2 target genes while CBR-470-1 does not (Figure 5C,D). However, both compounds induce activation of the OSR target gene *HMOX1* (Figure 5E). This result is identical to that observed by our targeted RNAseq analysis (Figure S5B-D). These results show that CBR-470-1 shows increased selectivity for OSR activation relative to bardoxolone and demonstrates the utility for our targeted RNAseq assay to profile the selectivity of putative OSR activating compounds in clinical development.

Defining the Selectivity of HSR Activating Compounds by Targeted RNAseq. Previous high-throughput screening identified numerous compounds, including compounds A3, C1, D1, and F1 (Figure S6A), that activate a cell-based reporter of the HSR-associated transcription factor HSF1 in HeLa cells.[21] However, the selectivity of these compounds for the HSR remains to be fully defined. Previous reports show that these compounds not only preferentially induce expression of HSR target genes but also show mild induction of genes regulated by other stress pathways such as *BiP* (or *HSPA5*) regulated by ATF6 and *HMOX1* regulated by the OSR. We used our targeted RNAseq assay to define the selectivity of these putative HSF1 activating compounds for specific HSR activation. Our results show that compound A3 strongly induced the HSR gene set (Figure 6A) to a level comparable to that observed with dox-dependent cHSF1 activation (Figure 2B). Compounds C1, D1, and F1 also significantly induced the HSR gene set, albeit to a lower extent (Figure 6B−D). Administration of these compounds also induced expression of other stress-responsive genes. This was most evident with A3, which showed robust activation of select ISR and OSR target genes such as *ATF3* and *HMOX1*, respectively, without global activation of these pathways (Figure 6A). Similar results were observed for the other three compounds to lesser extents (Figure 6B−D). Interestingly, both *ATF3* and *HMOX1* have been shown to be transcriptionally induced following stress-independent activation of the HSR-associated transcription factor HSF1,[17] suggesting that their increased level of expression in response to compound treatment could, in part, reflect HSF1 activity.

To further define the selectivity of these HSR activating compounds for the HSR proteostasis transcriptional program in HEK293T cells, we performed whole transcriptome RNAseq (Table S4). Analysis of the top 100 most significantly altered transcripts in this whole transcriptome RNAseq data demonstrated that compound A3 induced the strongest effects on gene expression, consistent with our targeted RNAseq results (Figure 6E). Furthermore, performing the same correlation-based gene set analysis used for targeted RNAseq revealed an identical preferential activation of the HSR in this whole transcriptome data set (Figure S6B−I). Interestingly, comparing genes induced by A3 with those induced by a 43 °C heat shock[6] or dox-dependent cHSF1[17] activation demonstrated an overlap of ∼100 genes (Figure 6F), including many classical HSR proteostasis target genes such as *HSPA1A*, *DNAJB1*, and *CryAB* (Table S4). Importantly, all shared upregulated targets between A3 and heat shock are also found as shared targets with dox-dependent cHSF1. While this supports an A3-dependent induction of the HSR, there are many genes upregulated in the whole transcriptome data that are not upregulated by these other HSR activating insults. GO analysis reveals that most targets induced by treatment with A3 are involved in RNA polymerase II-dependent transcription (Figure 6G). This finding is consistent with recent studies indicating that apart from direct transcriptional upregulation, HSF1 may recruit factors that increase the rate of release of Pol II from its paused state in transcript promoter regions.[6] Thus, the altered expression of Pol II regulatory factors suggests that A3 could influence HSR activity by targeting RNA Pol II pause release. While the impact of A3 on RNA Pol II could limit the further development and usage of this compound as a chemical tool for defining HSR-dependent regulation of cellular proteostasis, these results demonstrate the potential for our targeted RNAseq assay to define the selectivity of prioritized compounds identified through reporter-based HTS for activating specific stress-responsive proteostasis pathways.

CONCLUDING REMARKS

The establishment of highly selective activators of stress-responsive signaling pathways provides unique opportunities to identify new roles for these pathways in regulating cellular physiology and defining their potential for correcting pathologic defects associated with diverse diseases. Here, we establish a medium-throughput targeted RNAseq assay that reports on the activation of predominant stress-responsive proteostasis pathways such as the HSR, OSR, ISR, and UPR. We demonstrate the potential for this approach to deconvolute the complex integration of stress-responsive signaling pathways in HEK293 cells treated with chemical genetic or pharmacologic perturbations. Furthermore, we show that this approach is suitable for defining the selectivity of putative activators of different stress-responsive signaling pathways. These results demonstrate that this assay provides new opportunities to improve screening efforts focused on establishing pharmacologic activators of stress-responsive signaling pathways by identifying compounds or classes with high selectivity earlier in the screening pipeline (i.e., after reporter-based HTS). Furthermore, this assay can be paired with medicinal chemistry to establish next-generation compounds with improved selectivity and/or potency through monitoring activation of specific pathway reporter gene sets as well as other complementary approaches such as transcription factor knockouts or pharmacologic inhibitors of stress-responsive pathways to validate the activation or inhibition of specific pathways observed upon pharmacologic treatment.

While we specifically focus on stress-responsive proteostasis pathways in human HEK293 cells (see Figure 1A), many of the genes included in our stress pathway gene sets are robustly activated across mammalian cell types. For example, we used these gene sets to show activation of stress signaling pathways in mouse embryonic fibroblasts treated with Tg or As(III) similar to that observed in HEK293 cells (Figure S7). This indicates that this approach can report on stress pathway activation in

DOI: 10.1021/acschembio.9b00134
ACS Chem. Biol. 2019, 14, 784−795

other models. However, these gene sets could easily be modified to improve reporting on stress pathway activation in other models. The flexibility of the targeted RNAseq platform allows inclusion or replacement of reporter genes to enhance the ability to accurately report on pathway activation in specific tissues or organisms, providing new opportunities to monitor stress pathway activity *in vivo* for efforts such as defining compound bioavailability and pharmacodynamics. This platform can additionally be expanded through the inclusion of additional gene sets reporting on the activation of other signaling pathways, further improving the ability of this approach to define compound selectivity at early stages of compound development. Ultimately, the targeted RNAseq assay and approach described herein will improve the establishment of pharmacologic activators of stress-responsive signaling by providing new opportunities to define compound specificity at an earlier stage in compound development.

METHODS

Materials and Reagents. Thapsigargin was purchased from Fisher Scientific (catalog no. 50-464-295). Tunicamycin was purchased from Cayman Chemical (catalog no. 11089-65-9). Oligomycin A was purchased from Sigma-Aldrich (catalog no. 75351). Paraquat was purchased from Sigma-Aldrich (catalog no. 36541). The following qPCR primers were used: Bag3 (3′-TGGGAGATCAAGATCGACCC-5′, 5′-GGGCCATTGGCAGAGGATG-3′), Hspa5 (3′-GCCTGTATTTCTAGACCTGCC-5′, 5′-TTCATCTTGCCAGCCAGTTG-3′), Hmox1 (3′-GAGTGTAAGGACCCATCGGA-5′, 5′-GCCAGCAACAAAGTGCAAG-3′), and RiboPro control (3′-CGTCGCCTCCTACCTGCT-5′, 5′-CCATTCAGCTCACTGATAACCTTG-3′).

Cell Lines and Treatments. Stable cell lines expressing inducible cHSF1, ATF6, and XBP1s were used as previously described to activate cHSF1, ATF6, and XBP1s transcription factors, respectively.[17,28] Cells types as listed in Table 2 were cultured in DMEM with 10% FBS, pen/strep, and glutamine at 37 °C and 5% CO_2 in Corning 96-well tissue culture plates. Cells were treated for the indicated durations (Table S2) with either chemical genetic activators or pharmacologics solubilized in dimethyl sulfoxide (DMSO); treatments were performed in triplicate.

RNA Extraction. RNA was extracted from HEK293T, HEK293^{Dax}, and HEK293^{TREX} using the Zymo Research ZR-96 Quick-RNA isolation kit by following the manufacturer's instructions. Briefly, cells were rinsed with DMSO prior to lysis, and samples were then cleared of particulate matter through centrifugation. The supernatant was then subjected to standard column purification steps, including an on-column DNase treatment, prior to RNA elution in DNase/RNase-free water.

Targeted RNAseq Library Preparation and Sequencing. Stress-responsive sequencing libraries were prepared using the Illumna TruSeq Targeted RNA Expression technology, with targeted probes selected to create a custom gene panel to report on stress-responsive transcripts across several signaling pathways. Briefly, 50 ng of intact total RNA was reverse transcribed into cDNA using ProtoScript II Reverse Transcriptase (25 °C for 5 min, 42 °C for 15 min, 95 °C for 10 min, and held at 4 °C), and the targeted oligo pool was hybridized in each sample (70 °C for 5 min, 68 °C for 1 min, 65 °C for 2.5 min, 60 °C for 2.5 min, 55 °C for 4 min, 50 °C for 4 min, 45 °C for 4 min, 40 °C for 4 min, 35 °C for 4 min, 30 °C for 4 min, and held at 30 °C). Hybridized products were washed using magnetic beads, extended, and amplified using i7 and i5 adapters (95 °C for 2 min, 28 cycles at 98 °C for 30 s, 62 °C for 30 s, and 72 °C for 60 s, followed by 72 °C for 5 min, and held at 10 °C). Libraries were cleaned and pooled prior to being loaded on the MiSeq desktop sequencer.

Alignment and Expression Analysis. Alignment of targeted RNAseq reads was performed using the Illumina TruSeq Targeted RNAseq software using the custom target manifest containing sequences of targeted region sequences. Alignment of whole transcriptome RNAseq data was done using DNAstar Lasergene SeqManPro to the GRCh37.p13 human genome reference assembly. Aligned counts from Targeted RNAseq were median normalized and $\log_2$ transformed prior to linear regression.

Whole Transcriptome RNAseq. HEK293T cells were treated with 10 μM A3, C1, D1, or F1 for 6 h prior to RNA isolation using the ZymoPure RNA-mini kit by following the manufacturer's instructions, including on-column DNase I treatment to remove contaminating genomic DNA. RNA was quantified by NanoDrop. Conventional RNAseq was conducted via BGI Americas on the BGI Proprietary platform, providing single-end 50 bp reads at 20 million reads per sample. Each condition was performed in triplicate.

Gene Expression Correlation Network Graph and Hierarchical Clustering. Raw count data from the triplicate RNAseq experiments for each condition were averaged, and Pearson correlation coefficients were calculated for each pair of genes. We created the gene expression correlation graph by representing each gene as a vertex and connecting the vertices for the genes that had correlation coefficients of $\geq$0.6. There were a few genes whose expression levels did not correlate with those of any other genes at this level. These genes were connected only to the gene with which they had the highest correlation coefficient to ensure that the network graph was fully connected. The hierarchical clustering of genes by expression pattern shown in Figure 1 was performed using the Euclidean distance between each gene's expression level correlation coefficients with all other genes as the distance metric and single-linkage clustering as the linkage criterion. Thus, two genes that have similar sets of correlation coefficients with all other genes were most likely to cluster together. The network graph and dendrogram in Figure 1 were produced using Mathematica 11.3.

Statistical Analysis. Values of the statistical significance of residual values from targeted RNAseq correlation analysis were calculated using standard one-way ANOVA, with the lowest p values presented. Full ANOVA tables from our targeted RNAseq assay are included (Table S3). qPCR data were analyzed using a one-tailed Student's t test.

ASSOCIATED CONTENT

Supporting Information

The Supporting Information is available free of charge on the ACS Publications website at DOI: 10.1021/acschembio.9b00134.

Supplemental experimental procedures, figure legends for Figures S1−S7, Figures S1−S7, supplemental table legends for Tables S1−S5, and Table S3 (PDF)
Table S1 (XLSX)
Table S2 (XLSX)
Table S4 (XLSX)
Table S5 (XLSX)

AUTHOR INFORMATION

Corresponding Author

*Department of Molecular Medicine, The Scripps Research Institute, La Jolla, CA 92037. E-mail: wiseman@scripps.edu. Phone: (858) 784-8820.

ORCID

Lars Plate: 0000-0003-4363-6116
Michael J. Bollong: 0000-0001-9439-1476
R. Luke Wiseman: 0000-0001-9287-6840

Notes

The authors declare no competing financial interest.

ACKNOWLEDGMENTS

The authors thank S. Head, J. Shimashita, J. Kelly, and J. Rosarda at The Scripps Research Institute for fruitful discussions and experimental support related to the work described herein. This work was supported by National Institutes of Health Grants AG046495 (R.L.W.), DK106582 (E.T.P.), and GM101644

DOI: 10.1021/acschembio.9b00134
ACS Chem. Biol. 2019, 14, 784−795

(E.T.P.) and a Career Development Program Fellow Grant from the Leukemia and Lymphoma Society (Grant 5439-16 to L.P.).

REFERENCES

(1) Hetz, C., and Mollereau, B. (2014) Disturbance of endoplasmic reticulum proteostasis in neurodegenerative diseases. *Nat. Rev. Neurosci. 15*, 233−249.
(2) Henning, R. H., and Brundel, B. (2017) Proteostasis in cardiac health and disease. *Nat. Rev. Cardiol. 14*, 637−653.
(3) James, H. A., O'Neill, B. T., and Nair, K. S. (2017) Insulin Regulation of Proteostasis and Clinical Implications. *Cell Metab. 26*, 310−323.
(4) Wang, S., and Kaufman, R. J. (2012) The impact of the unfolded protein response on human disease. *J. Cell Biol. 197*, 857−867.
(5) Wang, M., and Kaufman, R. J. (2016) Protein misfolding in the endoplasmic reticulum as a conduit to human disease. *Nature 529*, 326−335.
(6) Mahat, D. B., Salamanca, H. H., Duarte, F. M., Danko, C. G., and Lis, J. T. (2016) Mammalian Heat Shock Response and Mechanisms Underlying Its Genome-wide Transcriptional Regulation. *Mol. Cell 62*, 63−78.
(7) Li, J., Labbadia, J., and Morimoto, R. I. (2017) Rethinking HSF1 in Stress, Development, and Organismal Health. *Trends Cell Biol. 27*, 895−905.
(8) Gomez-Pastor, R., Burchfiel, E. T., and Thiele, D. J. (2017) Regulation of heat shock transcription factors and their roles in physiology and disease. *Nat. Rev. Mol. Cell Biol. 19*, 4−19.
(9) Gorrini, C., Harris, I. S., and Mak, T. W. (2013) Modulation of oxidative stress as an anticancer strategy. *Nat. Rev. Drug Discovery 12*, 931−947.
(10) Taguchi, K., Motohashi, H., and Yamamoto, M. (2011) Molecular mechanisms of the Keap1-Nrf2 pathway in stress response and cancer evolution. *Genes Cells 16*, 123−140.
(11) Alam, J., Stewart, D., Touchard, C., Boinapally, S., Choi, A. M., and Cook, J. L. (1999) Nrf2, a Cap'n'Collar transcription factor, regulates induction of the heme oxygenase-1 gene. *J. Biol. Chem. 274*, 26071−26078.
(12) Walter, P., and Ron, D. (2011) The unfolded protein response: from stress pathway to homeostatic regulation. *Science 334*, 1081−1086.
(13) Han, J., and Kaufman, R. J. (2017) Physiological/pathological ramifications of transcription factors in the unfolded protein response. *Genes Dev. 31*, 1417−1438.
(14) Young, S. K., and Wek, R. C. (2016) Upstream open reading frames differentially regulate gene-specific translation in the integrated stress response. *J. Biol. Chem. 291*, 16927−16935.
(15) Donnelly, N., Gorman, A. M., Gupta, S., and Samali, A. (2013) The eIF2alpha kinases: their structures and functions. *Cell. Mol. Life Sci. 70*, 3493−3511.
(16) Pakos-Zebrucka, K., Koryga, I., Mnich, K., Ljujic, M., Samali, A., and Gorman, A. M. (2016) The integrated stress response. *EMBO Rep. 17*, 1374−1395.
(17) Ryno, L. M., Genereux, J. C., Naito, T., Morimoto, R. I., Powers, E. T., Shoulders, M. D., and Wiseman, R. L. (2014) Characterizing the altered cellular proteome induced by the stress-independent activation of heat shock factor 1. *ACS Chem. Biol. 9*, 1273−1283.
(18) Lu, P. D., Jousse, C., Marciniak, S. J., Zhang, Y., Novoa, I., Scheuner, D., Kaufman, R. J., Ron, D., and Harding, H. P. (2004) Cytoprotection by pre-emptive conditional phosphorylation of translation initiation factor 2. *EMBO J. 23*, 169−179.
(19) Lamech, L. T., and Haynes, C. M. (2015) The unpredictability of prolonged activation of stress response pathways. *J. Cell Biol. 209*, 781−787.
(20) Chen, J. J., Genereux, J. C., and Wiseman, R. L. (2015) Endoplasmic reticulum quality control and systemic amyloid disease: Impacting protein stability from the inside out. *IUBMB Life 67*, 404−413.
(21) Calamini, B., Silva, M. C., Madoux, F., Hutt, D. M., Khanna, S., Chalfant, M. A., Saldanha, S. A., Hodder, P., Tait, B. D., Garza, D., Balch, W. E., and Morimoto, R. I. (2012) Small-molecule proteostasis regulators for protein conformational diseases. *Nat. Chem. Biol. 8*, 185−196.
(22) Balch, W. E., Morimoto, R. I., Dillin, A., and Kelly, J. W. (2008) Adapting proteostasis for disease intervention. *Science 319*, 916−919.
(23) Cuadrado, A., Manda, G., Hassan, A., Alcaraz, M. J., Barbas, C., Daiber, A., Ghezzi, P., Leon, R., Lopez, M. G., Oliva, B., Pajares, M., Rojo, A. I., Robledinos-Anton, N., Valverde, A. M., Guney, E., and Schmidt, H. (2018) Transcription Factor NRF2 as a Therapeutic Target for Chronic Diseases: A Systems Medicine Approach. *Pharmacol. Rev. 70*, 348−383.
(24) Plate, L., and Wiseman, R. L. (2017) Regulating Secretory Proteostasis through the Unfolded Protein Response: From Function to Therapy. *Trends Cell Biol. 27*, 722−737.
(25) Sweeney, P., Park, H., Baumann, M., Dunlop, J., Frydman, J., Kopito, R., McCampbell, A., Leblanc, G., Venkateswaran, A., Nurmi, A., and Hodgson, R. (2017) Protein misfolding in neurodegenerative diseases: implications and strategies. *Transl. Neurodegener. 6*, 6.
(26) Plate, L., Cooley, C. B., Chen, J. J., Paxman, R. J., Gallagher, C. M., Madoux, F., Genereux, J. C., Dobbs, W., Garza, D., Spicer, T. P., Scampavia, L., Brown, S. J., Rosen, H., Powers, E. T., Walter, P., Hodder, P., Wiseman, R. L., and Kelly, J. W. (2016) Small molecule proteostasis regulators that reprogram the ER to reduce extracellular protein aggregation. *eLife 5*, e15550.
(27) Chiang, W. C., Messah, C., and Lin, J. H. (2012) IRE1 directs proteasomal and lysosomal degradation of misfolded rhodopsin. *Mol. Biol. Cell 23*, 758−770.
(28) Shoulders, M. D., Ryno, L. M., Genereux, J. C., Moresco, J. J., Tu, P. G., Wu, C., Yates, J. R., 3rd, Su, A. I., Kelly, J. W., and Wiseman, R. L. (2013) Stress-independent activation of XBP1s and/or ATF6 reveals three functionally diverse ER proteostasis environments. *Cell Rep. 3*, 1279−1292.
(29) Bollong, M. J., Lee, G., Coukos, J. S., Yun, H., Zambaldo, C., Chang, J. W., Chin, E. N., Ahmad, I., Chatterjee, A. K., Lairson, L. L., Schultz, P. G., and Moellering, R. E. (2018) A metabolite-derived protein modification integrates glycolysis with KEAP1-NRF2 signalling. *Nature 562*, 600−604.
(30) Flaherty, D. P., Miller, J. R., Garshott, D. M., Hedrick, M., Gosalia, P., Li, Y., Milewski, M., Sugarman, E., Vasile, S., Salaniwal, S., Su, Y., Smith, L. H., Chung, T. D., Pinkerton, A. B., Aube, J., Callaghan, M. U., Golden, J. E., Fribley, A. M., and Kaufman, R. J. (2014) Discovery of Sulfonamidebenzamides as Selective Apoptotic CHOP Pathway Activators of the Unfolded Protein Response. *ACS Med. Chem. Lett. 5*, 1278−1283.
(31) Kudo, T., Kanemoto, S., Hara, H., Morimoto, N., Morihara, T., Kimura, R., Tabira, T., Imaizumi, K., and Takeda, M. (2008) A molecular chaperone inducer protects neurons from ER stress. *Cell Death Differ. 15*, 364−375.
(32) Salehi, A. H., Morris, S. J., Ho, W. C., Dickson, K. M., Doucet, G., Milutinovic, S., Durkin, J., Gillard, J. W., and Barker, P. A. (2006) AEG3482 is an antiapoptotic compound that inhibits Jun kinase activity and cell death through induced expression of heat shock protein 70. *Chem. Biol. 13*, 213−223.
(33) Westerheide, S. D., Bosman, J. D., Mbadugha, B. N., Kawahara, T. L., Matsumoto, G., Kim, S., Gu, W., Devlin, J. P., Silverman, R. B., and Morimoto, R. I. (2004) Celastrols as inducers of the heat shock response and cytoprotection. *J. Biol. Chem. 279*, 56053−56060.
(34) Yang, H., Chen, D., Cui, Q. C., Yuan, X., and Dou, Q. P. (2006) Celastrol, a triterpene extracted from the Chinese "Thunder of God Vine," is a potent proteasome inhibitor and suppresses human prostate cancer growth in nude mice. *Cancer Res. 66*, 4758−4765.
(35) Trott, A., West, J. D., Klaic, L., Westerheide, S. D., Silverman, R. B., Morimoto, R. I., and Morano, K. A. (2008) Activation of heat shock and antioxidant responses by the natural product celastrol: transcriptional signatures of a thiol-targeted molecule. *Mol. Biol. Cell 19*, 1104−1112.
(36) Pronk, T. E., van der Veen, J. W., Vandebriel, R. J., van Loveren, H., de Vink, E. P., and Pennings, J. L. (2014) Comparison of the molecular topologies of stress-activated transcription factors HSF1, AP-

DOI: 10.1021/acschembio.9b00134
ACS Chem. Biol. 2019, 14, 784−795

1, NRF2, and NF-kappaB in their induction kinetics of HMOX1. *BioSystems 124*, 75−85.
(37) Ye, C., Ho, D. J., Neri, M., Yang, C., Kulkarni, T., Randhawa, R., Henault, M., Mostacci, N., Farmer, P., Renner, S., Ihry, R., Mansur, L., Keller, C. G., McAllister, G., Hild, M., Jenkins, J., and Kaykas, A. (2018) DRUG-seq for miniaturized high-throughput transcriptome profiling in drug discovery. *Nat. Commun. 9*, 4307.
(38) Martin, D. P., Miya, J., Reeser, J. W., and Roychowdhury, S. (2016) Targeted RNA Sequencing Assay to Characterize Gene Expression and Genomic Alterations. *J. Visualized Exp.*, DOI: 10.3791/54090.
(39) Koltai, H., and Weingarten-Baror, C. (2008) Specificity of DNA microarray hybridization: characterization, effectors and approaches for data correction. *Nucleic Acids Res. 36*, 2395−2405.
(40) Holtz, Y., Ardisson, M., Ranwez, V., Besnard, A., Leroy, P., Poux, G., Roumet, P., Viader, V., Santoni, S., and David, J. (2016) Genotyping by Sequencing Using Specific Allelic Capture to Build a High-Density Genetic Map of Durum Wheat. *PLoS One 11*, No. e0154609.
(41) Reeser, J. W., Martin, D., Miya, J., Kautto, E. A., Lyon, E., Zhu, E., Wing, M. R., Smith, A., Reeder, M., Samorodnitsky, E., Parks, H., Naik, K. R., Gozgit, J., Nowacki, N., Davies, K. D., Varella-Garcia, M., Yu, L., Freud, A. G., Coleman, J., Aisner, D. L., and Roychowdhury, S. (2017) Validation of a Targeted RNA Sequencing Assay for Kinase Fusion Detection in Solid Tumors. *J. Mol. Diagn. 19*, 682−696.
(42) Martinez-Jacobo, L., Ancer-Arellano, C. I., Ortiz-Lopez, R., Salinas-Santander, M., Villarreal-Villarreal, C. D., Ancer-Rodriguez, J., Camacho-Zamora, B., Zomosa-Signoret, V., Medina-De la Garza, C. E., Ocampo-Candiani, J., and Rojas-Martinez, A. (2018) Evaluation of the Expression of Genes Associated with Inflammation and Apoptosis in Androgenetic Alopecia by Targeted RNA-Seq. *Skin Appendage Disord 4*, 268−273.
(43) Hayes, J. D., and Dinkova-Kostova, A. T. (2014) The Nrf2 regulatory network provides an interface between redox and intermediary metabolism. *Trends Biochem. Sci. 39*, 199−218.
(44) Lee, A. H., Iwakoshi, N. N., and Glimcher, L. H. (2003) XBP-1 regulates a subset of endoplasmic reticulum resident chaperone genes in the unfolded protein response. *Mol. Cell. Biol. 23*, 7448−7459.
(45) Yamamoto, K., Sato, T., Matsui, T., Sato, M., Okada, T., Yoshida, H., Harada, A., and Mori, K. (2007) Transcriptional induction of mammalian ER quality control proteins is mediated by single or combined action of ATF6alpha and XBP1. *Dev. Cell 13*, 365−376.
(46) Harding, H. P., Zhang, Y., Zeng, H., Novoa, I., Lu, P. D., Calfon, M., Sadri, N., Yun, C., Popko, B., Paules, R., Stojdl, D. F., Bell, J. C., Hettmann, T., Leiden, J. M., and Ron, D. (2003) An integrated stress response regulates amino acid metabolism and resistance to oxidative stress. *Mol. Cell 11*, 619−633.
(47) Dengler, V. L., Galbraith, M., and Espinosa, J. M. (2014) Transcriptional regulation by hypoxia inducible factors. *Crit. Rev. Biochem. Mol. Biol. 49*, 1−15.
(48) Raskatov, J. A., Meier, J. L., Puckett, J. W., Yang, F., Ramakrishnan, P., and Dervan, P. B. (2012) Modulation of NF-kappaB-dependent gene transcription using programmable DNA minor groove binders. *Proc. Natl. Acad. Sci. U. S. A. 109*, 1023−1028.
(49) Zhao, Q., Wang, J., Levichkin, I. V., Stasinopoulos, S., Ryan, M. T., and Hoogenraad, N. J. (2002) A mitochondrial specific stress response in mammalian cells. *EMBO J. 21*, 4411−4419.
(50) Aldridge, J. E., Horibe, T., and Hoogenraad, N. J. (2007) Discovery of genes activated by the mitochondrial unfolded protein response (mtUPR) and cognate promoter elements. *PLoS One 2*, No. e874.
(51) Melber, A., and Haynes, C. M. (2018) UPR(mt) regulation and output: a stress response mediated by mitochondrial-nuclear communication. *Cell Res. 28*, 281−295.
(52) Kim, J. M., Kim, H. G., and Son, C. G. (2018) Tissue-Specific Profiling of Oxidative Stress-Associated Transcriptome in a Healthy Mouse Model. *Int. J. Mol. Sci. 19*, 3174.
(53) Miao, L., and St. Clair, D. K. (2009) Regulation of superoxide dismutase genes: implications in disease. *Free Radical Biol. Med. 47*, 344−356.
(54) Richard, E., Desviat, L. R., Ugarte, M., and Perez, B. (2013) Oxidative stress and apoptosis in homocystinuria patients with genetic remethylation defects. *J. Cell. Biochem. 114*, 183−191.
(55) Leclerc, D., and Rozen, R. (2008) Endoplasmic reticulum stress increases the expression of methylenetetrahydrofolate reductase through the IRE1 transducer. *J. Biol. Chem. 283*, 3151−3160.
(56) Druwe, I. L., and Vaillancourt, R. R. (2010) Influence of arsenate and arsenite on signal transduction pathways: an update. *Arch. Toxicol. 84*, 585−596.
(57) Qureshi, M. A., Haynes, C. M., and Pellegrino, M. W. (2017) The mitochondrial unfolded protein response: Signaling from the power-house. *J. Biol. Chem. 292*, 13500−13506.
(58) Chin, M. P., Bakris, G. L., Block, G. A., Chertow, G. M., Goldsberry, A., Inker, L. A., Heerspink, H. J. L., O'Grady, M., Pergola, P. E., Wanner, C., Warnock, D. G., and Meyer, C. J. (2018) Bardoxolone Methyl Improves Kidney Function in Patients with Chronic Kidney Disease Stage 4 and Type 2 Diabetes: Post-Hoc Analyses from Bardoxolone Methyl Evaluation in Patients with Chronic Kidney Disease and Type 2 Diabetes Study. *Am. J. Nephrol. 47*, 40−47.
(59) Yore, M. M., Kettenbach, A. N., Sporn, M. B., Gerber, S. A., and Liby, K. T. (2011) Proteomic analysis shows synthetic oleanane triterpenoid binds to mTOR. *PLoS One 6*, No. e22862.
(60) Gibellini, L., Pinti, M., Bartolomeo, R., De Biasi, S., Cormio, A., Musicco, C., Carnevale, G., Pecorini, S., Nasi, M., De Pol, A., and Cossarizza, A. (2015) Inhibition of Lon protease by triterpenoids alters mitochondria and is associated to cell death in human cancer cells. *Oncotarget 6*, 25466−25483.
(61) Huang, D. W., Sherman, B. T., Tan, Q., Collins, J. R., Alvord, W. G., Roayaei, J., Stephens, R., Baseler, M. W., Lane, H. C., and Lempicki, R. A. (2007) The DAVID Gene Functional Classification Tool: a novel biological module-centric algorithm to functionally analyze large gene lists. *Genome Biol. 8*, R183.

DOI: 10.1021/acschembio.9b00134
ACS Chem. Biol. 2019, 14, 784−795